

Decay of dark and bright plasmonic modes in a metallic nanoparticle dimerAdam Brandstetter-Kunc, Guillaume Weick,^{*} Dietmar Weinmann, and Rodolfo A. Jalabert*Institut de Physique et Chimie des Matériaux de Strasbourg, Université de Strasbourg, CNRS UMR 7504, F-67034 Strasbourg, France*

(Received 24 July 2014; revised manuscript received 20 November 2014; published 22 January 2015)

We develop a general quantum theory of the coupled plasmonic modes resulting from the near-field interaction between localized surface plasmons in a heterogeneous metallic nanoparticle dimer. In particular, we provide analytical expressions for the frequencies and decay rates of the bright and dark plasmonic modes. We show that, for sufficiently small nanoparticles, the main decay channel for the dark plasmonic mode, which is weakly coupled to light and, hence, immune to radiation damping, is of nonradiative origin and corresponds to Landau damping, i.e., decay into electron-hole pairs.

DOI: [10.1103/PhysRevB.91.035431](https://doi.org/10.1103/PhysRevB.91.035431)

PACS number(s): 73.20.Mf, 73.22.Lp, 78.67.Bf

I. INTRODUCTION

It has taken 74 years between the founding work of Mie on the optical response of a metallic nanoparticle [1] and the extension of Ruppin to the case of two nearby spheres [2]. At the practical level, the evolution from the single object to compound optical resonant systems has been even slower than the corresponding theoretical development. About twenty centuries span from the realization of optically active materials based on noninteracting nanoparticles [3] to the success in the fabrication and optical measurements of ensembles of interacting nanoparticles [4]. Nonetheless, once the theoretical and experimental basis for studying these compound objects was laid down, the subsequent developments have been extremely fast. In the field of nanoplasmonics [5], the intense recent activity concerning nanoparticle dimers [6] stems from the fact that it is the simplest system sustaining coupled plasmonic excitations.

The near-field interaction between the localized surface plasmons (LSPs) of two nanoparticles results in a bright mode (coupled to the electromagnetic field associated with visible light) and a dark one (weakly coupled to light). Both of these modes have been experimentally observed [6–12] and theoretically investigated [2,13–19]. On the one hand, the bright mode has been observed using laser excitation in various experimental systems [6–9]. On the other hand, the dark mode is difficult to excite in symmetric, homogeneous dimers with interparticle distance much smaller than the laser wavelength. However, this difficulty is less severe in heterogeneous dimers. The alternative experimental technique of electron energy loss spectroscopy (EELS) has recently provided an unambiguous detection of the dark mode [10–12].

The damping of these coupled modes is a crucial limiting factor for their experimental observation as well as for potential applications in the field of nanoplasmonics [5]. While the bright mode radiates in the far field and hence has a radiative decay, the dark mode is obviously immune to radiation damping. It is then of paramount interest to understand the nonradiative decay channels at the origin of the experimentally observed finite linewidth of the dark mode [10–12].

In this work we show that for dimers composed of sufficiently small nanoparticles, the main decay channel for the

dark mode corresponds to Landau damping, which dominates over absorption losses. In the present context, the Landau damping is a purely quantum-mechanical effect that leads to the decay of the collective excitation through the creation of electron-hole pairs [20,21]. Thus, we develop a general quantum theory of coupled plasmonic excitations in a heterogeneous dimer of metallic nanoparticles. Using bosonic Bogoliubov transformations and semiclassical techniques, we provide analytical expressions for the frequencies and lifetimes of the coupled plasmonic modes.

The present paper is organized as follows: Section II presents our model that we use in Secs. III and IV to obtain the frequencies and the decay rates of the coupled plasmonic modes, respectively. We draw our conclusions in Sec. V. The technical details of our calculations are presented in the appendixes.

II. OPEN QUANTUM SYSTEM APPROACH

For a single metallic nanoparticle, the separation of the electronic coordinates into center-of-mass and relative motion [22,23] amounts to a description typical for an open quantum system. The dipolar LSP (i.e., the center-of-mass coordinate) is coupled to an electronic environment (i.e., the bath of electron-hole pairs represented by the relative coordinates) and leads to the nonradiative decay of the collective excitation (Landau damping). The coupling between the two subsystems is a consequence of the breaking of Kohn's theorem [24,25] due to the nonharmonicity of the confining potential, the latter arising from the positive ionic background. In addition, radiative damping arises from the coupling of the LSP with electromagnetic field modes, while absorption (Ohmic) losses occur due to the finite resistivity of the metal.

As detailed in Appendix A, extending this approach to the case of a nanoparticle dimer (sketched in Fig. 1), the resulting electronic Hamiltonian can be written as

$$H = H_{\text{pl}} + H_{\text{eh}} + H_{\text{pl-eh}}. \quad (1)$$

The plasmonic part reads

$$H_{\text{pl}} = \sum_{n=1}^2 \hbar \tilde{\omega}_n b_n^\dagger b_n + \hbar \Omega f(\theta) (b_1^\dagger b_2 + b_1^\dagger b_2^\dagger + \text{H.c.}), \quad (2)$$

where the index n is used to identify within the dimer the two spherical, neutral nanoparticles of radius a_n (each containing

^{*}guillaume.weick@ipcms.unistra.fr

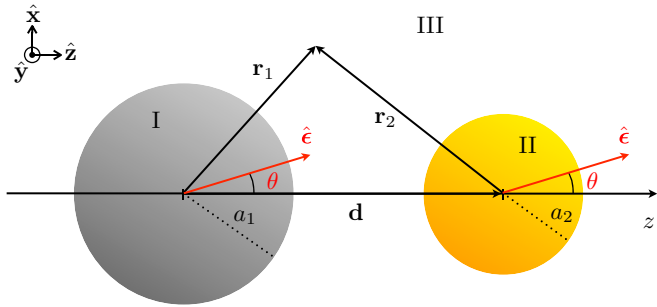


FIG. 1. (Color online) Sketch of a nanoparticle dimer formed by two spherical nanoparticles of radii a_1 and a_2 separated by a distance d , together with the coordinate system used in the text. The polarization $\hat{\epsilon}$ of the localized surface plasmons forming an angle θ with the z axis is also shown.

N_n electrons). The LSP frequency

$$\tilde{\omega}_n = \omega_n \sqrt{1 - \frac{N_{\text{out},n}}{N_n}}, \quad \omega_n = \sqrt{\frac{3N_n e^2}{m_e a_n^3 (\epsilon_d^{(n)} + 2\epsilon_m)}} \quad (3)$$

is redshifted with respect to the Mie frequency ω_n due to the $N_{\text{out},n}$ electrons spilling out of nanoparticle n [4]. Here, $-e$ and m_e denote the electron charge and mass, respectively. The dielectric constant $\epsilon_d^{(n)}$ takes into account the screening provided, in the case of noble metals, by the d electrons in nanoparticle n , and ϵ_m is the dielectric constant of the matrix in which the nanoparticles are embedded. In Eq. (2), the bosonic operator b_n (b_n^\dagger) annihilates (creates) an LSP in nanoparticle n [26]. The two LSPs interact through their near fields, giving rise to the second term in the right-hand side of Eq. (2), where

$$\Omega = \frac{1}{2} \prod_{n=1}^2 \left(\frac{\tilde{\omega}_n}{1 - N_{\text{out},n}/N_n} \right)^{1/2} \left(\frac{a_n}{d} \right)^{3/2} \quad (4)$$

and

$$f(\theta) = 1 - 3 \cos^2 \theta. \quad (5)$$

Here, d is the center-to-center nanoparticle distance and θ is the angle formed by the polarization $\hat{\epsilon}$ of the LSPs and the z axis joining the two NPs (see Fig. 1). In writing Eq. (2), we adopted a quasistatic dipole-dipole approximation valid for $3a_n \lesssim d \ll c/\tilde{\omega}_n$, where c is the speed of light [27,28]. We further assumed that in each eigenmode, the two LSPs are polarized in the same direction $\hat{\epsilon}$.

Electron-hole excitations within each nanoparticle provide the electronic environment described by [23]

$$H_{\text{ch}} = \sum_{n=1}^2 \sum_{\alpha} \varepsilon_{n\alpha} c_{n\alpha}^\dagger c_{n\alpha}, \quad (6)$$

where $c_{n\alpha}$ ($c_{n\alpha}^\dagger$) annihilates (creates) an electron in the n th nanoparticle associated with the one-body state $|n\alpha\rangle$ with energy $\varepsilon_{n\alpha}$ in the self-consistent potential V . Note that the form (6) implicitly assumes that tunneling of electrons between the two nanoparticles is suppressed. Similarly to the case of a single nanoparticle discussed above, the coupling of the plasmon to the electronic environment comes from the

nonharmonicity of the single-particle confinement, which in the jellium approximation with $\epsilon_d^{(n)} = \epsilon_m = 1$ reads

$$U_n(r_n) = \frac{N_n e^2}{2a_n^3} (r_n^2 - 3a_n^2) \Theta(a_n - r_n) - \frac{N_n e^2}{r_n} \Theta(r_n - a_n), \quad (7)$$

where r_n is the radial coordinate with respect to the center of nanoparticle n . Hence, the Hamiltonian $H_{\text{pl-ch}}$ in Eq. (1) can be written as

$$H_{\text{pl-ch}} = \sum_{n,n',n''=1}^2 \sqrt{\frac{\hbar}{2N_n m_e \tilde{\omega}_n}} (b_n + b_n^\dagger) \times \sum_{\alpha\beta} \langle n'\alpha | \hat{\epsilon} \cdot \nabla U_n(r_n) | n''\beta \rangle c_{n'\alpha}^\dagger c_{n''\beta}. \quad (8)$$

III. FREQUENCIES OF THE COUPLED PLASMONIC MODES

The quadratic Hamiltonian (2) representing the two coupled LSPs is diagonalized as

$$H_{\text{pl}} = \sum_{\sigma=\pm} \hbar \omega_\sigma B_\sigma^\dagger B_\sigma \quad (9)$$

by introducing the bosonic operators

$$B_\pm = \sum_{n=1}^2 (u_{n,\pm} b_n + \bar{u}_{n,\pm} b_n^\dagger). \quad (10)$$

For the general case of unequal frequencies $\tilde{\omega}_n$, following Tsallis' prescription for Bogoliubov transformations [29], we find (see Appendix B for details)

$$\omega_\pm = \sqrt{\frac{\tilde{\omega}_1^2 + \tilde{\omega}_2^2}{2} \pm \sqrt{4\Omega^2 \tilde{\omega}_1 \tilde{\omega}_2 f^2(\theta) + \left(\frac{\tilde{\omega}_1^2 - \tilde{\omega}_2^2}{2} \right)^2}} \quad (11)$$

and

$$u_{n,\pm} = [\pm \text{sgn}\{f(\theta)\}]^{n-1} \frac{\omega_\pm + \tilde{\omega}_n}{2\sqrt{\tilde{\omega}_n \omega_\pm}} \sqrt{\frac{\omega_\pm^2 - \tilde{\omega}_n^2}{2\omega_\pm^2 - \tilde{\omega}_1^2 - \tilde{\omega}_2^2}}, \quad (12a)$$

$$\bar{u}_{n,\pm} = [\pm \text{sgn}\{f(\theta)\}]^{n-1} \frac{\omega_\pm - \tilde{\omega}_n}{2\sqrt{\tilde{\omega}_n \omega_\pm}} \sqrt{\frac{\omega_\pm^2 - \tilde{\omega}_n^2}{2\omega_\pm^2 - \tilde{\omega}_1^2 - \tilde{\omega}_2^2}}. \quad (12b)$$

In Eqs. (12a) and (12b), $\hat{n} = 1(2)$ for $n = 2(1)$.

The two plasmonic eigenmodes correspond to the coherent oscillation of the two LSPs. For $\theta = 0$, the low-energy (high-energy) mode with frequency ω_- (ω_+) can be thought of as the in-phase (antiphase) motion of the two LSPs. Vice versa, for $\theta = \pi/2$, the $-$ and $+$ modes correspond to the antiphase and in-phase motions, respectively. Figure 2(a) shows the transition between these two previous extreme cases as a function of the polarization angle θ . In the special case $\tilde{\omega}_1 = \tilde{\omega}_2$ [i.e., identical nanoparticles, thin solid and dashed lines in Fig. 2(a)], the in-phase mode (with nonvanishing dipole moment) can be excited by dipolar light and thus receives the name of ‘‘bright mode.’’ It corresponds to the $-$ ($+$) eigenmode for polarization angles $\theta < (>)\theta_0$, where $\theta_0 = \arccos(1/\sqrt{3})$ is the angle for which the dipole-dipole interaction in Eq. (2)

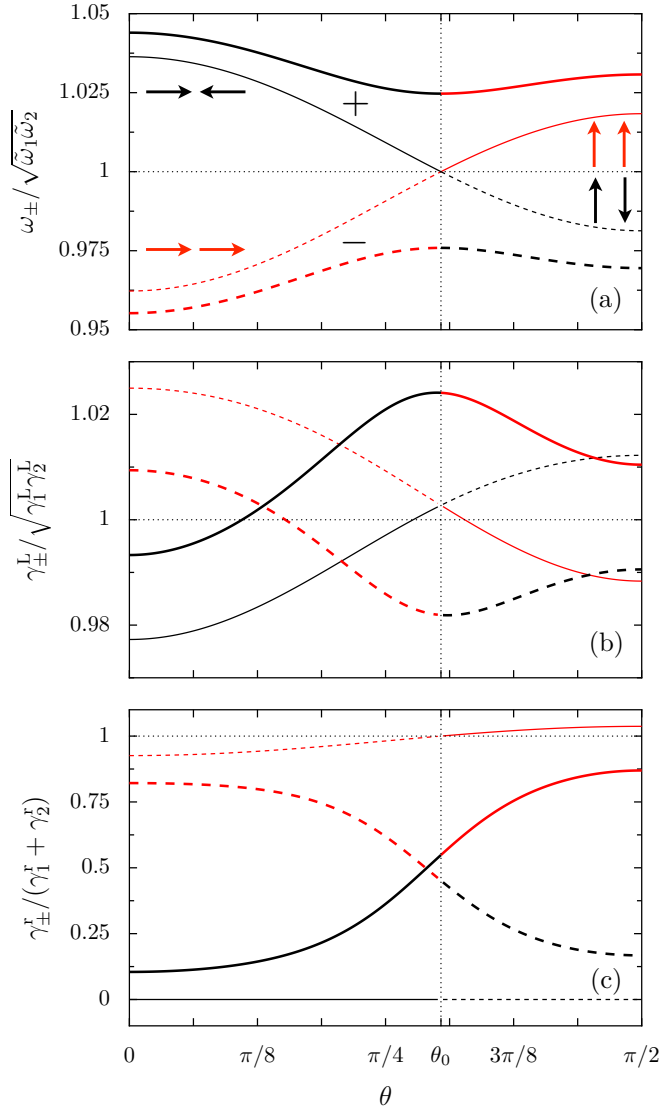


FIG. 2. (Color online) (a) Frequencies ω_{\pm} [Eq. (11)], (b) Landau damping linewidths γ_{\pm}^L [Eq. (22)], and (c) radiative damping linewidths γ_{\pm}^r [Eq. (26)] of the + (solid lines) and - (dashed lines) coupled plasmonic modes as a function of the polarization angle θ for $\tilde{\omega}_1/\tilde{\omega}_2 = 1$ (thin lines) and $\tilde{\omega}_1/\tilde{\omega}_2 = 1.05$ (thick lines). The bright (dark) modes for which the two LSPs are in phase (in antiphase) are represented by red/gray (black) curves. In the figure, the parameters are $a_1 = a_2 = a$, $d = 3a$, $\hbar\tilde{\omega}_1/E_F^{(1)} = 1$, and spillout is neglected.

vanishes. Conversely, the antiphase mode (with vanishing dipole moment) corresponds to the + (−) eigenmode for $\theta < (>)\theta_0$. Since it cannot be triggered by visible light, it is referred to as the “dark mode.” When $\tilde{\omega}_1 \neq \tilde{\omega}_2$ [thick, solid and dashed lines in Fig. 2(a)], the difference between bright and dark modes is less stringent, as both the + and − modes have a finite dipole moment for any θ . In this case the usage of bright (dark) modes refers to the larger (smaller) total dipole moment. Notice, moreover, that the dependence on the interparticle distance d of the \pm frequencies is encapsulated in Eq. (11) in the definition (4) of Ω , so that $\omega_{\pm} - [(\tilde{\omega}_1^2 + \tilde{\omega}_2^2)/2]^{1/2} \sim \pm 1/d^3$ [30]. Such a behavior, which directly follows from the form of the dipole-dipole

interaction, has also been unveiled both theoretically [2,14] and experimentally [8] in the case of nanoparticles of equal size and formed of the same material.

IV. NONRADIATIVE AND RADIATIVE DECAY RATES OF THE DARK AND BRIGHT MODES

A. Landau damping

The modes previously described can be understood as resulting from the coupling of classical dipoles, as has been extensively discussed in the literature [2,4,6–16]. Our quantum description is nevertheless crucial for the evaluation of the Landau damping of the two coupled plasmonic modes. The coupling Hamiltonian (8) associated with this decay channel can be expressed in terms of the B_{\pm} bosonic operators given in Eq. (10) as

$$H_{\text{pl-eh}} = \sum_{n=1}^2 \sum_{\sigma=\pm} \Lambda_n (B_{\sigma} + B_{\sigma}^{\dagger}) \sum_{\alpha\beta} \hat{\epsilon} \cdot \mathbf{D}_{\alpha\beta,\sigma}^{(n)} c_{n\alpha}^{\dagger} c_{n\beta}, \quad (13)$$

with

$$\mathbf{D}_{\alpha\beta,\sigma}^{(n)} = \Delta u_{n,\sigma} \mathbf{d}_{\alpha\beta}^{(n)} + \frac{2\Omega}{\omega_n} \Delta u_{\hat{n},\sigma} [\mathbf{d}_{\alpha\beta}^{(n)} - 3(\mathbf{d}_{\alpha\beta}^{(n)} \cdot \hat{\mathbf{z}})\hat{\mathbf{z}}], \quad (14)$$

where $\Lambda_n = (\hbar m_e \omega_n^3 / 2N_n)^{1/2}$ and $\Delta u_{n,\sigma} = u_{n,\sigma} - \bar{u}_{n,\sigma}$. Equation (13) is obtained under the assumption that the self-consistent potential V is constant inside the nanoparticles and infinite outside. Such an assumption, which neglects the spillout, is justified by density functional calculations for the one-particle case [23], as well as for dimers [17]. Within this approximation, the dipole matrix elements entering Eq. (14) reads

$$\mathbf{d}_{\alpha\beta}^{(n)} = \left(\sum_{s=\pm 1} \mathcal{A}_{l_{\alpha}l_{\beta},s}^{m_{\alpha}m_{\beta}} \frac{\hat{\mathbf{x}} - is\hat{\mathbf{y}}}{\sqrt{2}} + \mathcal{A}_{l_{\alpha}l_{\beta},0}^{m_{\alpha}m_{\beta}} \hat{\mathbf{z}} \right) \mathcal{R}_n(E_{\alpha}, E_{\beta}), \quad (15)$$

where the radial part is given by [31]

$$\mathcal{R}_n(E_{\alpha}, E_{\beta}) = \frac{2\hbar^2}{m_e a_n} \frac{\sqrt{E_{\alpha}E_{\beta}}}{(E_{\alpha} - E_{\beta})^2}. \quad (16)$$

The angular part in Eq. (15) is expressed in terms of Wigner-3j symbols as [32]

$$\mathcal{A}_{l_{\alpha}l_{\beta},s}^{m_{\alpha}m_{\beta}} = (-1)^{m_{\alpha}+s} \sqrt{(2l_{\alpha}+1)(2l_{\beta}+1)} \times \begin{pmatrix} l_{\alpha} & l_{\beta} & 1 \\ 0 & 0 & 0 \end{pmatrix} \begin{pmatrix} l_{\alpha} & l_{\beta} & 1 \\ -m_{\alpha} & m_{\beta} & s \end{pmatrix}. \quad (17)$$

Notice that the angular momenta selection rules $l_{\alpha} = l_{\beta} \pm 1$ and $m_{\alpha} = m_{\beta}$ ($s = 0$) and $m_{\alpha} = m_{\beta} \pm 1$ ($s = \pm 1$) are encapsulated in the expression above.

The zero-temperature Fermi’s golden rule decay rate of the + and − plasmonic modes from the Landau damping channel is then given from Eq. (13) by

$$\gamma_{\pm}^L = \frac{2\pi}{\hbar} \sum_{n=1}^2 \sum_{eh} |\Lambda_n \mathbf{D}_{eh,\pm}^{(n)} \cdot \hat{\epsilon}|^2 \delta(\hbar\omega_{\pm} - E_e + E_h), \quad (18)$$

where $|ne\rangle$ and $|nh\rangle$ represent, respectively, electron and hole states in the self-consistent potential V for the n th nanoparticle.

The sum over e and h states is performed by introducing the density of states $\varrho_l^{(n)}(E)$ with fixed angular momentum l at energy E in nanoparticle n . The angular momentum selection rules from Eq. (17) lead to

$$\gamma_{\pm}^L = \frac{16\pi}{3\hbar m_e^2 \omega_{\pm}^4} \sum_{n=1}^2 \frac{\Lambda_n^2}{a_n^2} \mathcal{P}_{n,\pm}(\theta) \int_{\max\{E_F^{(n)}, \hbar\omega_{\pm}\}}^{E_F^{(n)} + \hbar\omega_{\pm}} dE E E_{\pm} \\ \times \sum_l \varrho_l^{(n)}(E) [(l+1)\varrho_{l+1}^{(n)}(E_{\pm}) + l\varrho_{l-1}^{(n)}(E_{\pm})], \quad (19)$$

with $E_{\pm} = E - \hbar\omega_{\pm}$ and where

$$\mathcal{P}_{n,\pm}(\theta) = \sin^2 \theta \left(\Delta u_{n,\pm} + \frac{2\Omega}{\omega_n} \Delta u_{\hat{n},\pm} \right)^2 \\ + \cos^2 \theta \left(\Delta u_{n,\pm} - \frac{4\Omega}{\omega_n} \Delta u_{\hat{n},\pm} \right)^2. \quad (20)$$

Here, $E_F^{(n)}$ ($v_F^{(n)}$) stands for the Fermi energy (velocity) in nanoparticle n . Using the semiclassical leading-order form [33] of the density of states,

$$\varrho_l^{(n)}(E) \simeq \frac{\sqrt{2m_e a_n^2 E / \hbar^2 - (l+1/2)^2}}{2\pi E}, \quad (21)$$

the Landau damping decay rates read

$$\gamma_{\pm}^L = \sum_{n=1}^2 \frac{3v_F^{(n)}}{4a_n} \left(\frac{\omega_n}{\omega_{\pm}} \right)^3 g(\hbar\omega_{\pm}/E_F^{(n)}) \mathcal{P}_{n,\pm}(\theta), \quad (22)$$

where an explicit expression of the function

$$g(\nu) = \frac{2}{\nu} \int_{\max\{1,\nu\}}^{1+\nu} dx \int_0^{x-\nu} dy \sqrt{(x-y)(x-y-\nu)} \quad (23)$$

can be found in Refs. [31,32], thus yielding an analytical expression for the Landau damping decay rates.

The linewidths from Eq. (22) are represented as a function of the polarization angle θ in Fig. 2(b) for the case $\tilde{\omega}_1/\tilde{\omega}_2 = 1$ (thin lines) and $\tilde{\omega}_1/\tilde{\omega}_2 = 1.05$ (thick lines). The dark (black) and bright modes (red/gray lines) show a modulation with respect to the Landau damping linewidth of isolated nanoparticles [20,31,33],

$$\gamma_n^L = \frac{3v_F^{(n)}}{4a_n} g(\hbar\omega_n/E_F^{(n)}), \quad (24)$$

used as normalization. This anisotropy represents a qualitative difference as compared to the single nanoparticle case, stemming from the nonlocality of the coupled plasmonic modes. The expected tunability of $\pm 2\%$ obtained for $d = 3a$ [Fig. 2(b)] should be detectable in optical experiments for the bright mode. When $\tilde{\omega}_1/\tilde{\omega}_2 = 1$, the higher energy $+$ mode is less damped than the lower-energy $-$ one. This energy dependence is analogous to the single nanoparticle case, where higher mode frequencies correspond to lower values of the damping rates [34,35].

B. Absorption losses and radiation damping

In order to assess the relevance of Landau damping, we have to quantify the additional damping mechanisms not described by the Hamiltonian (1). The absorption losses given by the bulk

conductivity of the metal lead to a size-independent decay rate γ^a (which has a weak frequency dependence). The radiation damping rate γ_{\pm}^r relates the power P_{\pm}^r radiated with the energy E_{\pm} stored in the mode \pm as

$$P_{\pm}^r = \gamma_{\pm}^r E_{\pm}. \quad (25)$$

In the limit where the interparticle distance is much smaller than the wavelength associated with each LSP [36], one has $P_{\pm}^r = 2\omega_{\pm}^4 p_{\pm}^2/3c^3$, where p_{\pm} is the dipole moment corresponding to the \pm mode oscillating at the frequency ω_{\pm} given by Eq. (11). Averaging Eq. (25) on a period $2\pi/\omega_{\pm}$ much shorter than the decay time $1/\gamma_{\pm}^r$ leads to

$$\gamma_{\pm}^r = \frac{2\omega_{\pm}^3}{3c^3} \left(\sum_{n=1}^2 \sqrt{\tilde{\omega}_n a_n^3} \Delta u_{n,\pm} \right)^2. \quad (26)$$

The radiation damping linewidths above are shown in Fig. 2(c) as a function of polarization for $\tilde{\omega}_1/\tilde{\omega}_2 = 1$ (thin lines) and $\tilde{\omega}_1/\tilde{\omega}_2 = 1.05$ (thick lines). The normalization factor $\gamma_1^r + \gamma_2^r$ used in the figure corresponds to the radiation damping of two independent nanoparticles, with

$$\gamma_n^r = \frac{2\tilde{\omega}_n^4 a_n^3}{3c^3}. \quad (27)$$

For $\tilde{\omega}_1/\tilde{\omega}_2 = 1$, the dark mode has a vanishing radiative linewidth [thin black curve in Fig. 2(c)] as it does not couple to the electromagnetic field, while the radiation damping of the bright mode can be modulated with the light polarization (thin red/gray curve). Choosing $\tilde{\omega}_1/\tilde{\omega}_2 \neq 1$ opens the way to the optical detection of the dark mode, as its linewidth becomes finite [thick black curve in Fig. 2(c)].

C. Discussion

The relative importance of the three above-described damping mechanisms, as well as those arising from the nature of the embedding matrix (chemical interface damping and conduction band in the matrix [4]), depends on a variety of physical parameters that should be settled in order to achieve a meaningful comparison. We focus from now on on noble-metal nanoparticles [37], since they constitute the dimers experimentally studied [6–12]. We show in Fig. 3 the competition of γ_{\pm}^L and γ_{\pm}^r of the bright (light gray/red lines) and dark (black lines) plasmonic modes as a function of nanoparticle radius a (assumed to be the same for both particles) for homogeneous [Ag-Ag, Fig. 3(a)] and heterogeneous [Ag-Au, Fig. 3(b)] dimers with $d = 3a$. A matrix with $\epsilon_m = 4$ is assumed, which leads to LSP resonances $\omega_{\text{Ag}} = 2.6 \text{ eV}/\hbar$ and $\omega_{\text{Au}} = 2.2 \text{ eV}/\hbar$ [4]. We consider the transverse polarization ($\theta = \pi/2$), so that the $+$ ($-$) mode corresponds to the bright (dark) mode (see Fig. 2). As can be seen from Fig. 3(a), for the bright mode the Landau damping [Eq. (22) scaling with the nanoparticle size as $1/a$, solid line] dominates over radiation damping [Eq. (26) scaling as a^3 , dashed-dotted line] for $a \lesssim 15 \text{ nm}$. On the contrary, for the dark mode, Landau damping [dotted line in Fig. 3(a)] dominates for sizes up to which it becomes negligible as compared to the absorption losses, since the radiative contribution to the linewidth vanishes [see dashed line in Fig. 3(a)]. In the case of a heterogeneous dimer [Fig. 3(b)], the difference between the bright and dark

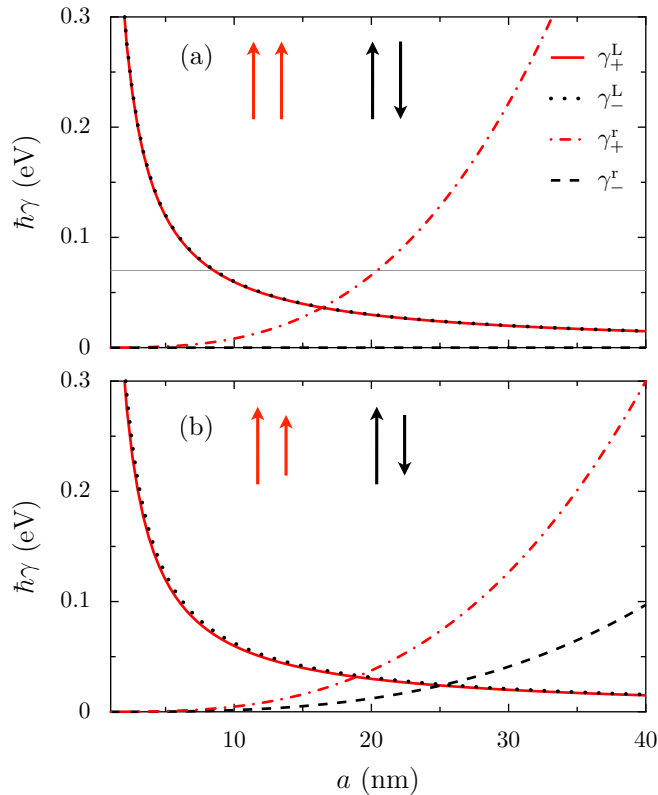


FIG. 3. (Color online) Landau damping (solid and dotted lines) and radiation damping (dashed-dotted and dashed lines) linewidths for transverse polarization $\theta = \pi/2$ as a function of nanoparticle radius a of the bright (+, light gray/red lines) and dark (–, black lines) mode. (a) Homogeneous dimer composed of two Ag nanoparticles. The thin gray line in the figure corresponds to the absorption losses measured in Ref. [38]. (b) Heterogeneous Ag-Au dimer. In the figure, $d = 3a$ and $\epsilon_m = 4$.

plasmonic modes is less stringent, as the dark mode acquires a finite dipole moment due to the difference in sizes and/or in densities between the two nanoparticles.

The agreement of our analytical theory with microscopic numerical calculations [17] is excellent. Using the time-dependent local-density approximation for Ag dimers with $a = 1.2$ nm, $d = 3a$ and $\theta = 0$, a resonance linewidth of 0.43 eV is obtained, while the Landau damping mechanism, dominating in this regime, yields [Eq. (22)] $\hbar\gamma_-^L = 0.40$ eV.

The existing experimental data exhibit tendencies that are consistent with our theoretical calculations. In Ag dimers excited by EELS [11] the bright and dark modes have both an increasing damping rate when passing from homogeneous to heterogeneous dimers, due to the larger dipole moments of the latter and the fact that the inhomogeneous dimers are achieved by using larger nanoparticles. Homogeneous dimers with $a = 12$ nm have a larger damping rate for the bright mode than for the dark one, due to the radiation damping contribution on the former. However, a quantitative comparison of the damping rates is handicapped by the limited resolution (~ 0.2 eV) of these EELS experiments [39]. Another difficulty for the quantitative comparison with the experiment is that the employed nanoparticles are very close to each other, taking the setup outside the validity of the dipole-dipole approximation

used in our theoretical approach. Moreover, the absorption losses, estimated [38] to be about $\hbar\gamma^a \simeq 70$ meV in optically excited Ag nanoparticles [see the thin gray line in Fig. 3(a)], are expected to be considerably larger in EELS experiments. This is due to the strong heating induced by the electron beam that might explain the value of the observed [11] total linewidths (~ 0.5 eV). In addition, the nature and dielectric properties of the material coating the nanoparticles are not well controlled.

V. CONCLUSION

We have presented a general quantum theory of coupled plasmonic modes in a heterogeneous metallic nanoparticle dimer. We have provided analytical expressions for the frequencies, Landau damping, and radiative linewidths of these plasmonic modes. The role of nonradiative damping for collective excitations of interacting metallic nanoparticles has been explored and quantified. In particular, we have shown that the Landau damping is an unavoidable decay channel for the dark plasmonic mode consistent with the tendencies of the experimentally observed linewidths [10–12]. Our work should motivate systematic measurements for different particle sizes and constitutes a first step of crucial importance towards the understanding of the damping mechanisms limiting plasmon propagation in technologically promising quantum metamaterials based on one- and two-dimensional arrays of nanoparticles [5,40], such as the honeycomb lattice supporting chiral massless Dirac-like plasmons [41,42].

ACKNOWLEDGMENTS

We are grateful to J. A. Badán, W. L. Barnes, E. Mariani, R. E. Marotti, and F. Vallée for helpful discussions. We acknowledge financial support from Centre National de la Recherche Scientifique (CNRS) through the PICS program (Contract No. 6384 APAG) and from Agence Nationale de la Recherche (ANR) under Grant No. ANR-14-CE26-0005 Q-MetaMat.

APPENDIX A: MICROSCOPIC HAMILTONIAN OF A METALLIC NANOPARTICLE DIMER

In this appendix, we detail the derivation of the Hamiltonian (1), which describes the bright and dark plasmonic modes and their coupling to electron-hole excitations. Within the jellium model which replaces the ions by a homogeneous positively charged background, the electronic Hamiltonian describing the nanoparticle dimer sketched in Fig. 1 reads

$$\begin{aligned}
 H = & \sum_{n=1}^2 \sum_{i=1}^{N_n} \left[\frac{\mathbf{p}_{n,i}^2}{2m_e} + U_{2\text{NP}}(\rho_{n,i}) \right] \\
 & + \frac{e^2}{2} \sum_{n=1}^2 \sum_{i,j=1(j \neq i)}^{N_n} \frac{1}{|\rho_{n,i} - \rho_{n,j}|} \\
 & + e^2 \sum_{i=1}^{N_1} \sum_{j=2}^{N_2} \frac{1}{|\rho_{1,i} - \rho_{2,j}|}, \quad (\text{A1})
 \end{aligned}$$

with $\boldsymbol{\rho}_{n,i}$ the position of the i th electron belonging to the n th nanoparticle and $\mathbf{p}_{n,i}$ its momentum. Note that the Hamiltonian (A1) describes a nanoparticle dimer in vacuum ($\epsilon_m = 1$) in which the screening due to the d electrons is negligible ($\epsilon_d^{(n)} = 1$). The third and fourth terms in the right-hand side in Eq. (A1) represent, respectively, the intra- and interparticle electron-electron interaction. The single-particle confinement potential created by the two positively charged jellium spheres (with charge $+N_n e$, $n = 1, 2$) reads

$$U_{2\text{NP}}(\boldsymbol{\rho}) = \begin{cases} \frac{N_1 e^2}{2a_1} \left[\left(\frac{r_1}{a_1} \right)^2 - 3 \right] - \frac{N_2 e^2}{r_2}, & \boldsymbol{\rho} \in \text{I}, \\ \frac{N_2 e^2}{2a_2} \left[\left(\frac{r_2}{a_2} \right)^2 - 3 \right] - \frac{N_1 e^2}{r_1}, & \boldsymbol{\rho} \in \text{II}, \\ -\frac{N_1 e^2}{r_1} - \frac{N_2 e^2}{r_2}, & \boldsymbol{\rho} \in \text{III}, \end{cases} \quad (\text{A2})$$

where $\mathbf{r}_n = \boldsymbol{\rho} - \mathbf{d}_n$, with \mathbf{d}_n the location of the center of the n th particle. Here, regions I and II are, respectively, inside nanoparticle 1 and 2, and region III corresponds to the space outside both particles (see Fig. 1).

Assuming that the interparticle distance d is much larger than the nanoparticle radii a_n , we expand the Hamiltonian (A1) to 2nd order in r_n/d . Within this approximation, the expansion of the interparticle electron-electron interaction term entering Eq. (A1) yields

$$\begin{aligned} & e^2 \sum_{i=1}^{N_1} \sum_{j=2}^{N_2} \frac{1}{|\boldsymbol{\rho}_{1,i} - \boldsymbol{\rho}_{2,j}|} \\ & \simeq \frac{2e^2}{d} \sum_{i=1}^{N_1} \sum_{j=1}^{N_2} \left\{ 1 + \frac{(\mathbf{r}_{1,i} - \mathbf{r}_{2,j}) \cdot \hat{\mathbf{d}}}{d} \right. \\ & \quad \left. - \frac{(\mathbf{r}_{1,i} - \mathbf{r}_{2,j}) \cdot [\mathbf{r}_{1,i} - \mathbf{r}_{2,j} - 3\hat{\mathbf{d}}((\mathbf{r}_{1,i} - \mathbf{r}_{2,j}) \cdot \hat{\mathbf{d}})]}{2d^2} \right\}. \end{aligned} \quad (\text{A3})$$

Here, $\mathbf{r}_{n,i}$ denotes the position of the i th electron belonging to the n th nanoparticle relative to its center. Similarly, the expansion of the single-particle confinement (A2) yields

$$U_{2\text{NP}}(\boldsymbol{\rho}_{1,i}) \simeq U_1(r_{1,i}) - \frac{N_2 e^2}{d} \left\{ 1 + \frac{\mathbf{r}_{1,i} \cdot \hat{\mathbf{d}}}{d} - \frac{\mathbf{r}_{1,i} \cdot [\mathbf{r}_{1,i} - 3\hat{\mathbf{d}}(\mathbf{r}_{1,i} \cdot \hat{\mathbf{d}})]}{2d^2} \right\}, \quad (\text{A4a})$$

$$U_{2\text{NP}}(\boldsymbol{\rho}_{2,i}) \simeq U_2(r_{2,i}) - \frac{N_1 e^2}{d} \left\{ 1 - \frac{\mathbf{r}_{2,i} \cdot \hat{\mathbf{d}}}{d} - \frac{\mathbf{r}_{2,i} \cdot [\mathbf{r}_{2,i} - 3\hat{\mathbf{d}}(\mathbf{r}_{2,i} \cdot \hat{\mathbf{d}})]}{2d^2} \right\}, \quad (\text{A4b})$$

where U_n is the single-particle confinement of an isolated nanoparticle defined in Eq. (7), which is harmonic with the Mie frequency inside the nanoparticle and Coulomb-like outside [23,33]. Notice that $\omega_1 = \omega_2$ if the two nanoparticles are made of the same metal, i.e., they have the same electronic density.

Using Eqs. (A3) and (A4) to express Eq. (A1), we obtain the Hamiltonian

$$H = \sum_{n=1}^2 H_n + H_{d-d}, \quad (\text{A5})$$

up to an irrelevant constant. In Eq. (A5),

$$H_n = \sum_{i=1}^{N_n} \left[\frac{\mathbf{p}_{n,i}^2}{2m_e} + U_n(r_{n,i}) \right] + \frac{e^2}{2} \sum_{i,j=1(i \neq j)}^{N_n} \frac{1}{|\mathbf{r}_{n,i} - \mathbf{r}_{n,j}|} \quad (\text{A6})$$

represents the Hamiltonian of the isolated nanoparticle n [23,33], while

$$H_{d-d} = \frac{e^2}{d^3} \sum_{i=1}^{N_1} \sum_{j=1}^{N_2} [\mathbf{r}_{1,i} \cdot \mathbf{r}_{2,j} - 3(\mathbf{r}_{1,i} \cdot \hat{\mathbf{d}})(\mathbf{r}_{2,j} \cdot \hat{\mathbf{d}})] \quad (\text{A7})$$

stands for the dipole-dipole interaction between the two electron distributions in the respective nanoparticles. Note that retardation effects can be neglected as we assume that the interparticle distance d is much smaller than the wavelength associated with each LSP frequency, so that the quasistatic approximation is valid.

The Hamiltonian (A5) can be conveniently expressed in terms of the electronic center-of-mass coordinates $\mathbf{R}_n = \sum_{i=1}^{N_n} \mathbf{r}_{n,i}/N_n$ and momenta $\mathbf{P}_n = \sum_{i=1}^{N_n} \mathbf{p}_{n,i}$, and the relative coordinates $\mathbf{r}'_{n,i} = \mathbf{r}_{n,i} - \mathbf{R}_n$ and $\mathbf{p}'_{n,i} = \mathbf{p}_{n,i} - \mathbf{P}_n/N_n$ ($n = 1, 2$) [22,23]. Assuming that the center-of-mass displacements are much smaller than the nanoparticle radii, we obtain to second order in the parameter $R_n/a_n \ll 1$ the decomposition (1). The center-of-mass Hamiltonian representing the plasmonic collective excitations coupled via the dipole-dipole interaction reads

$$\begin{aligned} H_{\text{pl}} = & \sum_{n=1}^2 \left(\frac{P_n^2}{2M_n} + \frac{M_n}{2} \tilde{\omega}_n^2 R_n^2 \right) \\ & + \frac{Q_1 Q_2}{d^3} [\mathbf{R}_1 \cdot \mathbf{R}_2 - 3(\mathbf{R}_1 \cdot \hat{\mathbf{d}})(\mathbf{R}_2 \cdot \hat{\mathbf{d}})], \end{aligned} \quad (\text{A8})$$

with $M_n = N_n m_e$ and $Q_n = N_n e$ the total electronic mass and charge in the n th nanoparticle, respectively, and where $\tilde{\omega}_n$ is defined in Eq. (3). In Eq. (1),

$$\begin{aligned} H_{\text{eh}} = & \sum_{n=1}^2 \sum_{i=1}^{N_n} \left[\frac{p'_{n,i}{}^2}{2m_e} + U_n(r'_{n,i}) \right] \\ & + \frac{e^2}{2} \sum_{n=1}^2 \sum_{i,j=1(i \neq j)}^{N_n} \frac{1}{|\mathbf{r}'_{n,i} - \mathbf{r}'_{n,j}|} \end{aligned} \quad (\text{A9})$$

represents the Hamiltonian for the relative electronic coordinates, while

$$H_{\text{pl-ch}} = \sum_{n=1}^2 \sum_{i=1}^{N_n} \mathbf{R}_n \cdot \nabla U_n(r_{n,i}) \Big|_{\mathbf{R}_n=0} \quad (\text{A10})$$

is the coupling Hamiltonian between center-of-mass and relative coordinates.

Introducing the bosonic operator

$$b_n = \frac{1}{\sqrt{2}} \left(\frac{R_n}{\ell_n} + \frac{i P_n \ell_n}{\hbar} \right) \quad (\text{A11})$$

annihilating a plasmon in nanoparticle n and its adjoint b_n^\dagger , with $\ell_n = (\hbar/M_n \tilde{\omega}_n)^{1/2}$ the associated oscillator length, the plasmonic Hamiltonian (A8) transforms into Eq. (2). Notice that in writing the latter, we assumed that in each eigenmode the two LSPs are polarized in the same direction $\hat{\epsilon} = \cos \theta \hat{z} + \sin \theta \hat{x}$ forming an angle θ with the z axis (see Fig. 1).

Assuming that electronic correlations are not important for the present problem, we approximate the Hamiltonian (A9) by its mean-field counterpart (6). Density functional theory numerical calculations [17] suggest that the self-consistent potential V can be approximated by two spherical square wells of height V_0 centered around each nanoparticle,

$$V(\rho) \simeq \begin{cases} 0, & \rho \in \text{I} \ \& \ \text{II}, \\ V_0, & \rho \in \text{III}. \end{cases} \quad (\text{A12})$$

Note that the form (6) implicitly assumes that tunneling of electrons between the two wells is suppressed. Within our mean-field approximation, the coupling Hamiltonian (A10) thus takes the form (8). By relating collective and relative coordinates, this expression provides the way to calculate the decay rate of the coupled plasmonic modes within a quantum-mechanical approach.

The separation of center-of-mass and relative coordinates presented in this appendix allowed a complete quantum-mechanical treatment of the problem, which by essence is nonlocal. Notice that nonlocal effects in nanostructures can also be included within classical electrodynamic theories [43].

APPENDIX B: DIAGONALIZATION OF THE PLASMONIC HAMILTONIAN

The standard bosonic Bogoliubov transformation, applicable when the two oscillators have the same frequency, becomes more complicated in the case that interests us of a heterogeneous dimer. In this appendix, we follow Tsallis [29] for the diagonalization of the Hamiltonian (2). Towards this purpose, we introduce the operators

$$\mathbf{b} = \begin{pmatrix} b_1 \\ b_2 \\ b_1^\dagger \\ b_2^\dagger \end{pmatrix}, \quad \mathbf{b}^\dagger = (b_1^\dagger \quad b_2^\dagger \quad b_1 \quad b_2) \quad (\text{B1})$$

and

$$\mathbf{B} = \begin{pmatrix} B_+ \\ B_- \\ B_+^\dagger \\ B_-^\dagger \end{pmatrix} = \mathcal{T}^\dagger \mathbf{b}, \quad \mathbf{B}^\dagger = (B_+^\dagger \quad B_-^\dagger \quad B_+ \quad B_-) = \mathbf{b}^\dagger \mathcal{T}. \quad (\text{B2})$$

The transformation matrix \mathcal{T} is defined by

$$\mathcal{T} = \begin{pmatrix} u_{1,+} & u_{1,-} & \bar{u}_{1,+} & \bar{u}_{1,-} \\ u_{2,+} & u_{2,-} & \bar{u}_{2,+} & \bar{u}_{2,-} \\ \bar{u}_{1,+} & \bar{u}_{1,-} & u_{1,+} & u_{1,-} \\ \bar{u}_{2,+} & \bar{u}_{2,-} & u_{2,+} & u_{2,-} \end{pmatrix}, \quad (\text{B3})$$

so that $H_{\text{pl}} = \mathbf{b}^\dagger \mathcal{H}_{\text{pl}} \mathbf{b} = \mathbf{B}^\dagger \mathcal{H}_{\text{pl}}^{\text{D}} \mathbf{B}$ with

$$\mathcal{H}_{\text{pl}} = \frac{\hbar}{2} \begin{pmatrix} \tilde{\omega}_1 & \Omega f(\theta) & 0 & \Omega f(\theta) \\ \Omega f(\theta) & \tilde{\omega}_2 & \Omega f(\theta) & 0 \\ 0 & \Omega f(\theta) & \tilde{\omega}_1 & \Omega f(\theta) \\ \Omega f(\theta) & 0 & \Omega f(\theta) & \tilde{\omega}_2 \end{pmatrix} \quad (\text{B4})$$

and

$$\mathcal{H}_{\text{pl}}^{\text{D}} = \frac{\hbar}{2} \begin{pmatrix} \omega_+ & 0 & 0 & 0 \\ 0 & \omega_- & 0 & 0 \\ 0 & 0 & \omega_+ & 0 \\ 0 & 0 & 0 & \omega_- \end{pmatrix}, \quad (\text{B5})$$

up to irrelevant constants. Imposing that the new operators B_\pm of Eq. (B2) are bosonic, the coefficients entering the transformation matrix \mathcal{T} defined in Eq. (B3) obey

$$\sum_{n=1}^2 (u_{n,\pm}^2 - \bar{u}_{n,\pm}^2) = 1. \quad (\text{B6})$$

Obtaining the diagonal form (B5) amounts to diagonalizing the matrix $2\mathcal{H}_{\text{pl}}\mathcal{J}$, where

$$\mathcal{J} = \begin{pmatrix} 1 & 0 & 0 & 0 \\ 0 & 1 & 0 & 0 \\ 0 & 0 & -1 & 0 \\ 0 & 0 & 0 & -1 \end{pmatrix}. \quad (\text{B7})$$

The condition $\det \{2\mathcal{H}_{\text{pl}}\mathcal{J} - \hbar\omega\mathbb{1}\} = 0$ yields the eigenvalue equation

$$(\omega^2 - \tilde{\omega}_1^2)(\omega^2 - \tilde{\omega}_2^2) = 4\Omega^2 \tilde{\omega}_1 \tilde{\omega}_2 f^2(\theta). \quad (\text{B8})$$

Solving for ω , we find the eigenfrequencies (11) of the coupled plasmonic modes. The eigenvectors of $2\mathcal{H}_{\text{pl}}\mathcal{J}$ then determine the coefficients of the transformation matrix (B3) through

$$\begin{pmatrix} \tilde{\omega}_1 - \omega_\pm & \Omega f(\theta) & 0 & \Omega f(\theta) \\ \Omega f(\theta) & \tilde{\omega}_2 - \omega_\pm & \Omega f(\theta) & 0 \\ 0 & \Omega f(\theta) & -\tilde{\omega}_1 - \omega_\pm & -\Omega f(\theta) \\ \Omega f(\theta) & 0 & -\Omega f(\theta) & -\tilde{\omega}_2 - \omega_\pm \end{pmatrix} \times \begin{pmatrix} u_{1,\pm} \\ u_{2,\pm} \\ \bar{u}_{1,\pm} \\ \bar{u}_{2,\pm} \end{pmatrix} = 0. \quad (\text{B9})$$

Solving for the system (B9), we find together with the condition (B6) and with the help of the eigenvalue equation (B8) the coefficients (12) entering the transformation matrix (B3).

[1] G. Mie, Beiträge zur Optik trüber Medien, speziell kolloidaler Metallösungen, *Ann. Phys. (Leipzig)* **330**, 377 (1908).

[2] R. Ruppin, Surface modes of two spheres, *Phys. Rev. B* **26**, 3440 (1982).

- [3] I. Freestone, N. Meeks, M. Sax, and C. Higgitt, The Lycurgus cup: A Roman nanotechnology, *Gold Bull.* **40**, 270 (2007).
- [4] U. Kreibig and M. Vollmer, *Optical Properties of Metal Clusters* (Springer-Verlag, Berlin, 1995).
- [5] S. A. Maier, *Plasmonics: Fundamentals and Applications* (Springer-Verlag, Berlin, 2007).
- [6] P. K. Jain and M. A. El-Sayed, Plasmonic coupling in noble metal nanostructures, *Chem. Phys. Lett.* **487**, 153 (2010).
- [7] H. Tamaru, H. Kuwata, H. T. Miyazaki, and K. Miyano, Resonant light scattering from individual Ag nanoparticles and particle pairs, *Appl. Phys. Lett.* **80**, 1826 (2002).
- [8] W. Rechberger, A. Hohenau, A. Leitner, J. R. Krenn, B. Lamprecht, and F. R. Aussenegg, Optical properties of two interacting gold nanoparticles, *Opt. Commun.* **220**, 137 (2003).
- [9] P. Olk, J. Renger, M. T. Wenzel, and L. M. Eng, Distance dependent spectral tuning of two coupled metal nanoparticles, *Nano Lett.* **8**, 1174 (2008).
- [10] M.-W. Chu, V. Myroshnychenko, C. H. Chen, J.-P. Deng, C.-Y. Mou, and F. J. García de Abajo, Probing bright and dark surface-plasmon modes in individual and coupled noble metal nanoparticles using an electron beam, *Nano Lett.* **9**, 399 (2009).
- [11] A. L. Koh, K. Bao, I. Khan, W. E. Smith, G. Kothleitner, P. Nordlander, S. A. Maier, and D. W. McComb, Electron energy-loss spectroscopy (EELS) of surface plasmons in single silver nanoparticles and dimers: Influence of beam damage and mapping of dark modes, *ACS Nano* **3**, 3015 (2009).
- [12] S. J. Barrow, D. Rossouw, A. M. Funston, G. A. Botton, and P. Mulvaney, Mapping bright and dark modes in gold nanoparticle chains using electron energy loss spectroscopy, *Nano Lett.* **14**, 3799 (2014).
- [13] J. M. Gérardy and M. Ausloos, Absorption spectrum of clusters of spheres from the general solution of Maxwell's equations. IV. Proximity, bulk, surface, and shadow effects (in binary clusters), *Phys. Rev. B* **27**, 6446 (1983).
- [14] P. Nordlander, C. Oubre, E. Prodan, K. Li, and M. I. Stockman, Plasmon hybridization in nanoparticle dimers, *Nano Lett.* **4**, 899 (2004).
- [15] C. Dahmen, B. Schmidt, and G. von Plessen, Radiation damping in metal nanoparticle pairs, *Nano Lett.* **7**, 318 (2007).
- [16] G. Bachelier, I. Russier-Antoine, E. Benichou, C. Jonin, N. Del Fatti, F. Vallée, and P.-F. Brevet, Fano profiles induced by near-field coupling in heterogeneous dimers of gold and silver nanoparticles, *Phys. Rev. Lett.* **101**, 197401 (2008).
- [17] J. Zuloaga, E. Prodan, and P. Nordlander, Quantum description of the plasmon resonances of a nanoparticle dimer, *Nano Lett.* **9**, 887 (2009).
- [18] R. Esteban, A. G. Borisov, P. Nordlander, and J. Aizpurua, Bridging quantum and classical plasmonics with a quantum-corrected model, *Nat. Commun.* **3**, 825 (2012).
- [19] P. Zhang, J. Feist, A. Rubio, P. García-González, and F. J. García-Vidal, *Ab initio* nanoplasmonics: The impact of atomic structure, *Phys. Rev. B* **90**, 161407(R) (2014).
- [20] A. Kawabata and R. Kubo, Electronic properties of fine metallic particles. II. Plasma resonance absorption, *J. Phys. Soc. Jpn.* **21**, 1765 (1966).
- [21] G. F. Bertsch and R. A. Broglia, *Oscillations in Finite Quantum Systems* (Cambridge University Press, Cambridge, England, 1994).
- [22] L. G. Gerchikov, C. Guet, and A. N. Ipatov, Multiple plasmons and anharmonic effects in small metallic clusters, *Phys. Rev. A* **66**, 053202 (2002).
- [23] G. Weick, G.-L. Ingold, R. A. Jalabert, and D. Weinmann, Surface plasmon in metallic nanoparticles: Renormalization effects due to electron-hole excitations, *Phys. Rev. B* **74**, 165421 (2006).
- [24] W. Kohn, Cyclotron resonance and de Haas-van Alphen oscillations of an interacting electron gas, *Phys. Rev.* **123**, 1242 (1961).
- [25] L. Jacak, P. Hawrylak, and A. Wójs, *Quantum Dots* (Springer-Verlag, Berlin, 1998).
- [26] For the LSP quantization procedure in nanoparticles of arbitrary shape, see D. J. Bergman and M. I. Stockman, Surface plasmon amplification by stimulated emission of radiation: Quantum generation of coherent surface plasmons in nanosystems, *Phys. Rev. Lett.* **90**, 027402 (2003).
- [27] M. L. Brongersma, J. W. Hartman, and H. A. Atwater, Electromagnetic energy transfer and switching in nanoparticle chain arrays below the diffraction limit, *Phys. Rev. B* **62**, R16356 (2000).
- [28] S. Y. Park and D. Stroud, Surface-plasmon dispersion relations in chains of metallic nanoparticles: An exact quasistatic calculation, *Phys. Rev. B* **69**, 125418 (2004).
- [29] C. Tsallis, Diagonalization methods for the general bilinear Hamiltonian of an assembly of bosons, *J. Math. Phys.* **19**, 277 (1978).
- [30] This dependence on d strictly holds in the regime $|\tilde{\omega}_1^2 - \tilde{\omega}_2^2|/2\tilde{\omega}_1\tilde{\omega}_2 \ll 2\Omega|f(\theta)|/(\tilde{\omega}_1\tilde{\omega}_2)^{1/2} \ll 1$. In the case $2\Omega|f(\theta)|/(\tilde{\omega}_1\tilde{\omega}_2)^{1/2} \ll |\tilde{\omega}_1^2 - \tilde{\omega}_2^2|/2\tilde{\omega}_1\tilde{\omega}_2 \ll 1$, we have $\omega_+ \simeq \max\{\tilde{\omega}_1, \tilde{\omega}_2\}$ and $\omega_- \simeq \min\{\tilde{\omega}_1, \tilde{\omega}_2\}$.
- [31] C. Yannouleas and R. A. Broglia, Landau damping and wall dissipation in large metal clusters, *Ann. Phys. (NY)* **217**, 105 (1992).
- [32] G. Weick and D. Weinmann, Lifetime of the surface magneto-plasmons in metallic nanoparticles, *Phys. Rev. B* **83**, 125405 (2011).
- [33] G. Weick, R. A. Molina, D. Weinmann, and R. A. Jalabert, Lifetime of the first and second collective excitations in metallic nanoparticles, *Phys. Rev. B* **72**, 115410 (2005).
- [34] C. Seoanez, G. Weick, R. A. Jalabert, and D. Weinmann, Friction of the surface plasmon by high-energy particle-hole pairs, *Eur. Phys. J. D* **44**, 351 (2007).
- [35] Notice that even in the case where the dipole-dipole interaction vanishes ($\theta = \theta_0$), γ_{\pm}^L is not simply equal to the linewidth γ_n^L of an isolated nanoparticle defined in Eq. (24). This effect is due to the modification of the nonharmonic part of the single-particle confinement (7) by the other nanoparticle and the subsequent breaking of Kohn's theorem.
- [36] G. S. Smith, An insightful problem involving the electromagnetic radiation from a pair of dipoles, *Eur. J. Phys.* **31**, 819 (2010).
- [37] The Mie frequency defined in Eq. (3), depending on the dielectric constants inside and outside the nanoparticle, provides in general a good approximation to the experimentally obtained values (though deviations may appear in the presence of interband transitions close to the resonance frequency). The precise value of the Landau damping rate in noble metals is difficult to determine since in the case of very small nanoparticles, it depends on the softness of the self-consistent confining potential. This is

- due to the dielectric mismatch at the nanoparticle boundary; see Ref. [23].
- [38] K.-P. Charlé, W. Schulze, and B. Winter, The size dependent shift of the surface plasmon absorption band of small spherical metal particles, *Z. Phys. D* **12**, 471 (1989).
- [39] Notice that a considerably higher resolution (10 meV) within the EELS technique has been very recently reported in O. L. Krivanek, T. C. Lovejoy, N. Dellby, T. Aoki, R. W. Carpenter, P. Rez, E. Soignard, J. Zhu, P. E. Batson, M. J. Lagos, R. F. Egerton, and P. A. Crozier, Vibrational spectroscopy in the electron microscope, *Nature (London)* **514**, 209 (2014).
- [40] N. Meinzer, W. L. Barnes, and I. R. Hooper, Plasmonic meta-atoms and metasurfaces, *Nat. Photon.* **8**, 889 (2014).
- [41] G. Weick, C. Woollacott, W. L. Barnes, O. Hess, and E. Mariani, Dirac-like plasmons in honeycomb lattices of metallic nanoparticles, *Phys. Rev. Lett.* **110**, 106801 (2013).
- [42] T. J. Sturges, C. Woollacott, G. Weick, and E. Mariani, Dirac plasmons in bipartite lattices of metallic nanoparticles, [arXiv:1411.7796](https://arxiv.org/abs/1411.7796).
- [43] S. Raza, S. I. Bozhevolnyi, M. Wubs, and N. A. Mortensen, Nonlocal optical response in metallic nanostructures, [arXiv:1412.0942](https://arxiv.org/abs/1412.0942).